

Dufour and thermal diffusion effects on time-dependent natural MHD convective transport over an inclined porous plate

Md. Hasanuzzaman^{a,*}, Mahamudul Hassan Milon^a, Md. Mosharrof Hossain^b,
Md. Asaduzzaman^a

^a Department of Mathematics, Khulna University of Engineering & Technology, Khulna, 9203, Bangladesh

^b Department of Mathematics, Bangladesh University of Engineering & Technology, Dhaka, 1000, Bangladesh

ARTICLE INFO

Keywords:

Porosity
MHD
Dufour and thermal diffusion
Inclined porous plate

ABSTRACT

In this research article, we examined the influences of thermal diffusion and Dufour on time-dependent free MHD convective transport flow through an inclined permeable plate numerically. The dimensionless ordinary differential equations are found from the dimensional governing non-linear partial differential equations through the use of similarity transformation. The transformed dimensionless ordinary differential equations are resolved by employing the finite difference method in the Shooting technique through MATLAB software. The numerical outcomes have been presented for the impact of several non-dimensional numbers or parameters to explore the fluid flow, and heat and mass transfer features. The fluid velocity diminishes for mounting amounts of the inclined angle. The values of $f(0)$ go up by about 75 % due to rising values of the inclined angle from 15° to 60° . With other previously released research studies, a comparison has been performed. The present research reveals good agreement with the published study.

1. Introduction

A permeable medium flowing through a vertical sheet is common in nature. The porous medium has several inflections in science and engineering. The problem of natural magneto-convective heat–mass transport of an electrically conducting fluid over an inclined heated surface has drawn interest because of its application to many engineering problems, astrophysics, and geophysics for example the cooling towers, boundary layer control in aerodynamics, nuclear reactors cooling. Umemura and Law [1] presented the effect of an inclined angle on the natural convection boundary layer flow passing a flat sheet. They observed that the flow properties depend on the distance from the leading edge and the extent of inclination. The impacts of thermal radiation with free convection on the boundary layer movement from an inclined isothermal sheet have been examined by Hossain et al. [2]. Anghel et al. [3] explored the combined thermal and mass (concentration) properties on time-independent laminar free convection boundary layer fluid flow passing an inclined flat sheet. The influences of viscous dissipation and ohmic heating on MHD natural convection flow over an inclined porous plate have been examined by Chen [4]. In his simulation, he also took into account the fluctuating wall temperature and

concentration. Alam et al. [5] took into consideration the effect of heat generation on steady natural magneto-convective heat–mass transport over an inclined sheet. The impact of heat generation on steady 2D mass and heat transfer movement of a dissipating, electrically conducting incompressible fluid passing an inclined permeable plate has been examined by Reddy [6]. Magnetohydrodynamic (MHD) flow through an inclined porous sheet has a vital role in the fields of pure science, engineering, biomedical and technological sciences for example, electrolytes, blood flow measurements, metal-working processes, MHD power generators, control fusion research, propulsion units, MHD accelerators, ionized gases, and traveling wave tubes. An inclined sheet is a plate revolving concerning several angles over time. A porous plate is shown as a sheet with a porous surface. The rock and soil mechanics, petroleum technology, porous media, human lungs, material science, small blood capillaries, and the dying process consisting of the porous medium. Ali et al. [7] resolved the governing equations for a time-dependent MHD natural viscous convective transport along an inclined surface.

When the mass and heat transfers happen jointly in a continuous fluid, the driving potentials and fluxes have a more complicated relationship. In addition to composition gradients, temperature gradients can also result in an energy flux. The diffusion-thermo or Dufour impact can be defined as the energy flux created by a temperature gradient. The

* Corresponding author.

E-mail address: hasanuzzaman@math.kuet.ac.bd (Md. Hasanuzzaman).

Nomenclature			
MHD	hydromagnetic	S_h	Sherwood number
u	velocity component along the x-direction	v	uniform magnetic field
T	fluid temperature	B	velocity component along the y- direction
T_∞	free stream temperature	J	current density
T_w	wall temperature	$U_0(t)$	uniform surface velocity
T_m	fluid mean temperature	$v(t)$	suction velocity
C	fluid concentration	C_p	specific heat at constant pressure
C_w	wall concentration	ρ	fluid density
C_∞	free stream concentration	g	acceleration due to gravity
k	thermal conductivity	ν	kinematic viscosity
β^*	volumetric expansion coefficient including concentration	C_s	concentration susceptibility
σ	similarity parameter	β	volumetric expansion coefficient including temperature
D_m	mass diffusivity coefficient	ν_0	suction and blowing parameter
M	magnetic force parameter	k_T	thermal diffusion ratio
P_r	Prandtl number	G_r	local Grashof number
G_m	modified local Grashof number	D_f	Dafour number
t	time	S_r	Soret number
N_u	Nusselt number	S_c	Schmidt number
$f(\eta)$	dimensionless velocity	τ	Shear stress
		$\phi(\eta)$	dimensionless concentration
		$\theta(\eta)$	dimensionless temperature

mass fluxes may similarly be produced by concentration gradients. This concentration gradient is said to be the Soret effect or thermal diffusion. For example, mixing gases with extremely light molecular weights (H_2 , He) and isotope separation have both been accomplished using the Soret (thermal-diffusion) effect. According to Eckert and Drake [8], the Dufour (diffusion-thermo) impact was found to be of sufficient average molecular weight (N_2 , air) to not be disregarded. Following Dursunkaya and Worek [9], Kafoussias and Williams [10] explored the impacts of diffusion-thermo and thermal-diffusion on transient and constant natural convection from a vertical surface in light of the significance of the aforementioned effects. Later, Postelnicu [11] examined the Dufour and Soret influences on heat and mass transmission by free convection from vertical surfaces in permeable media with a chemical reaction effect. The effects of thermophoresis on MHD-free convective fluid flow with heat–mass transport along an inclined porous stretched sheet have been studied by Alam [12]. Along with concentration and wall temperature variations, they took into account the Soret and Dufour effects. Prabhakar and Makinde [13] examined the time-dependent MHD boundary layer flow of a radiating and reacting electrically conducting fluid past a slippery permeable vertical sheet embedded in a perforated medium. Sreedevi et al. [14] the effect of the radiative on MHD flow with heat and mass transfer past a permeable stretching sheet including the Soret and Dufour effects. Mondal et al. [15] investigated the influences of the Soret–Dufour and the thermophoresis on MHD convective transport of a semi-infinite permeable inclined flat sheet. They also considered the effects of non-uniform heat source/sink and chemical reaction in their simulations. The influence of the blowing/suction parameter on unstable free convection fluid movement through a vertical slender body has been explored by Hasanuzzaman et al. [16]. Recently, Hasanuzzaman et al. [17] observed the properties of thermal diffusion and Dufour impacts on time-dependent natural MHD convective heat–mass transmission over an infinite vertical porous sheet. With the aid of the ‘Tecplot’ software, they also applied the superposition approach to the ODE solutions. Later, by taking the additional terms thermal radiation and internal heat absorption or generation, respectively, Hasanuzzaman et al. [18,19] enhanced Hasanuzzaman et al. [17]. Their simulation is almost the same as our simulation. By taking into account the inclined porous plate in this article, we advanced the research of Hasanuzzaman et al. [17].

The goal of the existing research is to examine the time-dependent free magneto-convective heat–mass transmission movement over an

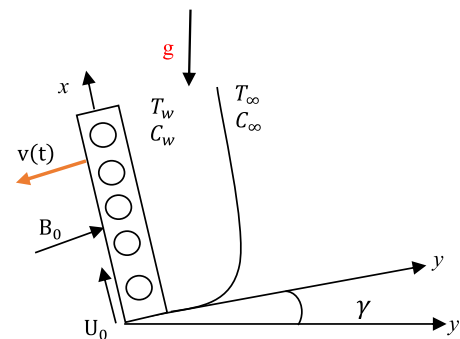


Fig. 1. Physical model and coordinate systems.

inclined porous plate. The key novelty of this study is improved further by assuming the inclined angle with finite difference method (FDM) which has not been explained yet. Another novelty of this paper is to compare our results with Hasanuzzaman et al. [17]. The FDM performs a suitable role in current research in this area. This method is a powerful technique to solve several types of problems. By using this technique, a set of algebraic equations is created from the provided ordinary differential equations. The resulting set of algebraic equations was resolved using the Newton iteration approach. The effect of several non-dimensional numbers or parameters on numbers for example inclined angle, Prandtl number, magnetic number, Soret number, Schmidt number, Dufour number, and suction parameter are explained graphically in this simulation. Moreover, the tabular formations have been exploited to clarify the properties of heat–mass transport and the skin friction coefficient.

2. Mathematical analysis

The two-dimensional time-dependent electrically conducting incompressible and viscous fluid flow passing an infinite inclined porous sheet is assumed. The infinite inclined porous sheet is taken along the x-axis. The inclined porous sheet is parallel to free-stream velocity. The inclined porous sheet is taken as perpendicular across the y-axis. The uniform magnetic field B_0 is applied along the flow direction (Pai [20]).

For $t > 0$, the wall concentration and temperature are C_w and T_w , respectively with velocity U_0 . The flow configuration along with coordinate systems are displayed in Fig. 1. The fluid is believed to have constant properties, with the body force term assuming just the effects of density fluctuations with concentration and temperature. The velocity components are considered to be the functions of y and t based only on the assumptions mentioned above.

Considering Boussinesq's approximation, we have the governing equations provided by (Hasanuzzaman et al. [14]):

The continuity equation-

$$\frac{\partial v}{\partial y} = 0 \quad (1)$$

The Momentum Equation:

$$\frac{\partial u}{\partial t} + v \frac{\partial u}{\partial y} = \nu \frac{\partial^2 u}{\partial y^2} + g\beta \cos\gamma (T - T_\infty) + g\beta^* \cos\gamma (C - C_\infty) - \frac{\sigma' B_0^2 u}{\rho} \quad (2)$$

The Energy Equation:

$$\frac{\partial T}{\partial t} + v \frac{\partial T}{\partial y} = \frac{k}{\rho C_p} \frac{\partial^2 T}{\partial y^2} + \frac{D_m k_T}{C_s C_p} \frac{\partial^2 C}{\partial y^2} \quad (3)$$

The Concentration Equation:

$$\frac{\partial C}{\partial t} + v \frac{\partial C}{\partial y} = D_m \frac{\partial^2 C}{\partial y^2} + \frac{D_m k_T}{T_m} \frac{\partial^2 T}{\partial y^2} \quad (4)$$

The associated boundary conditions are-

$$t > 0, u = U_0(t), v = v(t), T = T_w, C = C_w \text{ at } y = 0 \quad (5)$$

$$t > 0, u = 0, v = 0, T \rightarrow T_\infty, C \rightarrow C_\infty \text{ at } y \rightarrow \infty \quad (6)$$

where u and v are the respective velocity components across the x - and y -axes, γ is the inclined angle, t is the time, ν is the kinematic viscosity, T is the fluid temperature, g is the gravitational acceleration, β is the volumetric expansion coefficient due to temperature, C is the fluid concentration, T_∞ is the free stream fluid temperature, β^* is the expansion of the volumetric coefficient due to concentration, C_∞ is the free stream fluid concentration, T_w is the wall temperature, C_w is the wall concentration, k is the thermal conductivity of the sheet, ρ is the fluid density, C_p is the specific heat at constant pressure, C_s is the concentration susceptibility, D_m is the coefficient of the mass diffusivity, T_m is the mean temperature of the fluid, and k_T is the thermal diffusion ratio.

Using σ as a similarity parameter

$$\sigma = \sigma(t) \quad (7)$$

where the length scale is denoted by σ . This length is dependent on time. With this time-dependent length scale in consideration, the solution to continuity Eq. (1) is given by:

$$v = -v_0 \frac{v}{\sigma} \quad (8)$$

where the non-dimensional normal velocity at the sheet is v_0 . Here $v_0 < 0$ performs blowing and $v_0 > 0$ performs suction.

The similarity transformations are given by

$$\eta = \frac{y}{\sigma}, f(\eta) = \frac{u}{U_0}, \theta(\eta) = \frac{T - T_\infty}{T_w - T_\infty}, \phi(\eta) = \frac{C - C_\infty}{C_w - C_\infty} \quad (9)$$

Using the above Eqs. (7)–(9), the partial differential Eqs. (1)–(4) are changed into the following dimensionless coupled ODEs:

$$f'' + 2\xi f' + \cos\gamma G_r \theta + \cos\gamma G_m \phi - Mf = 0 \quad (10)$$

$$\theta'' + Pr(2\xi \theta' + D_f \phi') = 0 \quad (11)$$

$$\phi'' + 2\xi Sc \phi' + Sc S_c \theta' = 0 \quad (12)$$

subject to the boundary conditions

$$f = 1, \theta = 1, \phi = 1 \text{ at } \eta = 0 \quad (13)$$

$$f = 0, \theta = 0, \phi = 0 \text{ at } \eta \rightarrow \infty \quad (14)$$

where the Prandtl number is $Pr = \frac{\rho \nu C_p}{k}$, $G_m = \frac{g\beta^* (C_w - C_\infty) \sigma^2}{U_0 \nu}$ is the modified local Grashof number, the Magnetic force parameter is $M = \frac{\sigma' B_0^2 \sigma^2}{\rho \nu}$, the local Grashof number is $G_r = \frac{g\beta (T_w - T_\infty) \sigma^2}{U_0 \nu}$, the Soret number is $S_r = \frac{D_m k_T (T_w - T_\infty)}{\nu T_m (C_w - C_\infty)}$, the Dufour number is $D_f = \frac{D_m k_T (C_w - C_\infty)}{C_s C_p \nu (T_w - T_\infty)}$, the Schmidt number is $S_c = \frac{\nu}{D_m}$, and $\xi = \eta + \frac{v_0}{2}$ is the time-dependent parameter.

The Physical parameters are given by

$$Nu\alpha - \theta'(0), C_f = f'(0), Sh\alpha - \phi'(0) \quad (15)$$

where Nu represents the Nusselt number, C_f is the local skin friction, and Sh indicates the Sherwood number.

3. Numerical analysis

The major goal of this study is to employ the FDM to resolve a set of ODEs (10)–(12) connected to some boundary conditions (13) and (14). By Ali et al. [21], and Cheng and Liu [22], this kind of approach is operated to resolve a variety of problems accurately and effectively. FDMs are discretized from the solution's domain location.

We have taken the grid size in η -direction as $\Delta\eta = h > 0$, $\Delta\eta = \frac{1}{N}$, with $\eta_i = ih$ for $i = 0, 1, \dots, N$. Define $f_i = f(\eta_i)$, $\theta_i = \theta(\eta_i)$ and $\phi_i = \phi(\eta_i)$.

Let the numerical values of f , θ , and ϕ be F_i , Θ_i and Φ_i at the i th node, respectively. We have considered:

$$f'_i|_i = \frac{f_{i+1} - f_{i-1}}{2h}, \theta'_i|_i = \frac{\theta_{i+1} - \theta_{i-1}}{2h}, \phi'_i|_i = \frac{\phi_{i+1} - \phi_{i-1}}{2h} \quad (16)$$

$$f''_i|_i = \frac{f_{i+1} - 2f_i + f_{i-1}}{h^2}, \theta''_i|_i = \frac{\theta_{i+1} - 2\theta_i + \theta_{i-1}}{h^2}, \phi''_i|_i = \frac{\phi_{i+1} - 2\phi_i + \phi_{i-1}}{h^2} \quad (17)$$

The initial step is the application of FDM to discretize the set of ODEs (22)–(25) in space. We ignore the truncation errors and substitute (10)–(12) from (16) and (17). For ($i = 0, 1, \dots, N$), the following are the algebraic equations that are generated here:

$$F_{i+1} - 2F_i + F_{i-1} + \xi h(F_{i+1} - F_{i-1}) + \cos\gamma(G_r \Theta_i + G_c \Phi_i) - Mh^2 F_i = 0 \quad (18)$$

$$\Theta_{i+1} - 2\Theta_i + \Theta_{i-1} + Pr[\xi h(\Theta_{i+1} - \Theta_{i-1}) + D_f(\Phi_{i+1} - 2\Phi_i + \Phi_{i-1})] = 0 \quad (19)$$

$$\Phi_{i+1} - 2\Phi_i + \Phi_{i-1} + Sc[\xi h(\Phi_{i+1} - \Phi_{i-1}) + S_r(\Theta_{i+1} - 2\Theta_i + \Theta_{i-1})] = 0 \quad (20)$$

Also, the boundary conditions are

$$F_0 = 1, \Theta_0 = 1, \Phi_0 = 1, F_N = 0, \Theta_N = 0, \Phi_N = 0 \quad (21)$$

An algebraic system of nonlinear equations in F_i, Θ_i , and Φ_i is represented by the system of Eqs. (18)–(20) with the boundary conditions. Using the Newton iteration approach through 'MATLAB ODE45 software, the above equations have been resolved.

4. Results and discussions

The effects of thermal diffusion and Dufour on the time-dependent magneto-convective heat-mass transmission over a continuous porous sheet have been examined numerically. The coupled ODEs (10)–(12) are solved by inserting the FDM by the shooting technique using 'ODE45 MATLAB software. The dimensionless temperature, concentration, and velocity profiles are discussed for several amounts of the dimensionless parameters or numbers in this numerical calculation. In this paper, the

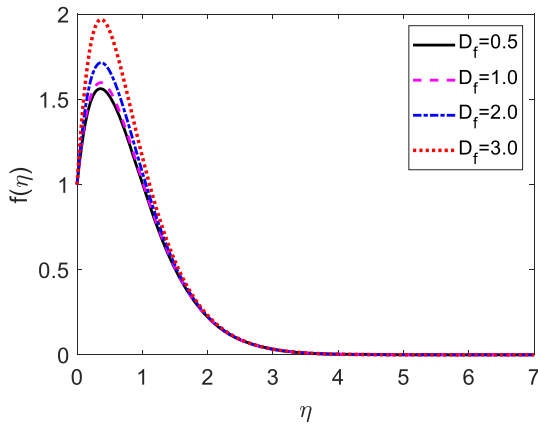


Fig. 2. Velocity profile for (D_f).

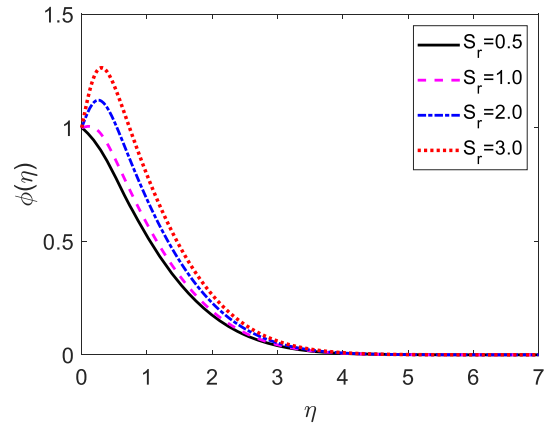


Fig. 5. Concentration profile for (S_r).

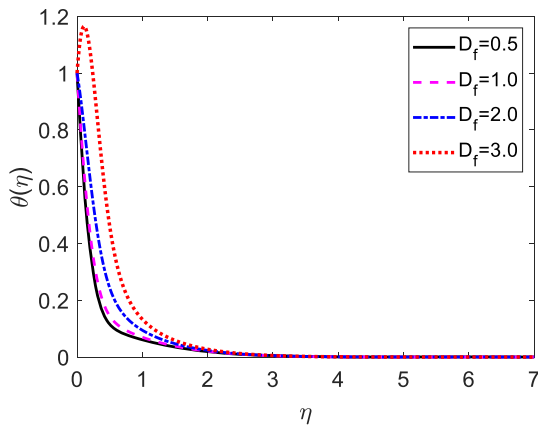


Fig. 3. Temperature profile for (D_f).

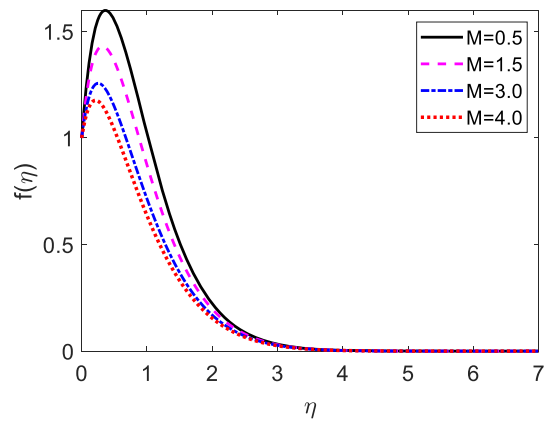


Fig. 6. Velocity profile for (M).

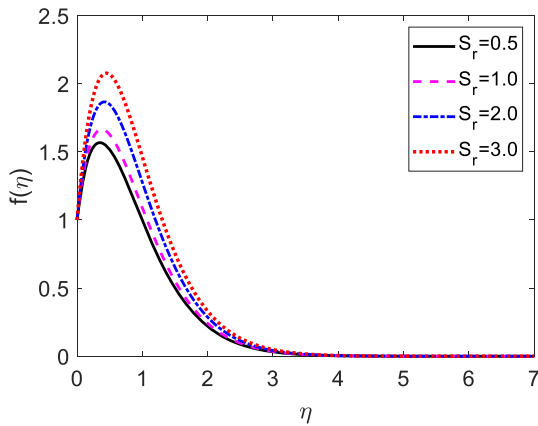


Fig. 4. Velocity profile for (S_r).

following non-dimensional parameters or numbers values are considered: $\gamma = 15^0, M = 0.5, D_f = 2.0, S_r = 2.0, Pr = 7.0, G_r = G_m = 10.0, Sc = 0.22$. Unless otherwise noted, all Figures are connected with these values.

The effect of the Dufour number (D_f) on the velocity and temperature fields is revealed in Figs. 2 and 3. The Dufour number is the ratio of thermal diffusion (k_T) and the kinematic viscosity (ν). The mathematical formula of the Dufour number is $D_f = \frac{D_m k_T (C_w - C_\infty)}{C_s C_p \nu (T_w - T_\infty)}$. From Fig. 2, it can be concluded that the kinematic viscosity lessens for moving amounts of D_f . It means that the fluid particles freely move in the computational

domain. Because of this, the fluid velocity improves for growing amounts of D_f . We can conclude from Fig. 3 that with uplifting amounts of D_f , the thermal diffusion improves. It means that the heat transmission rate reduces for rising amounts of D_f . It means that rising quantities of D_f cause to reduction in the heat transfer rate. Because of this, the fluid temperature improves for improving quantities of D_f . The influence of the potent Dufour effects is significantly accelerated by the thermal boundary layer thickness.

Figs. 4 and 5 present the velocity and concentration distributions for several quantities of the Soret number (S_r). It is well known that S_r is the ratio of the mass diffusivity coefficient (D_m) to the kinematic viscosity (ν). The mathematical formula for S_r is given by $S_r = \frac{D_m k_T (T_w - T_\infty)}{\nu T_m (C_w - C_\infty)}$. The kinematic viscosity (ν) has an inverse relationship with the Soret number. From Fig. 4, we can conclude that the kinematic viscosity lessens for improving values of S_r . Accordingly, improving quantities of S_r results in less friction force. This enables the fluid to move without restriction within the simulation domain. Hence the fluid velocity enhances for improving amounts of S_r . Also, the mass diffusivity coefficient (D_m) has the inverse relationship with the Soret number. Fig. 5 states that the mass diffusivity coefficient upsurges for improving amounts of S_r . When there is a differential between light and heavy molecules due to temperature gradient, the Soret effect develops. Then the mass transfer rate reduces. Hence, the fluid concentration improves for mounting quantities of S_r . Consequently, the concentration distribution is remarkably improved due to uprising amounts of S_r . To raise the concentration boundary layer thickness, this result is crucial.

The contribution of the magnetic force parameter (M) on the velocity profiles is demonstrated in Fig. 6. We have noticed from Fig. 6 that as the magnetic intensity enhances, the velocity field diminishes throughout

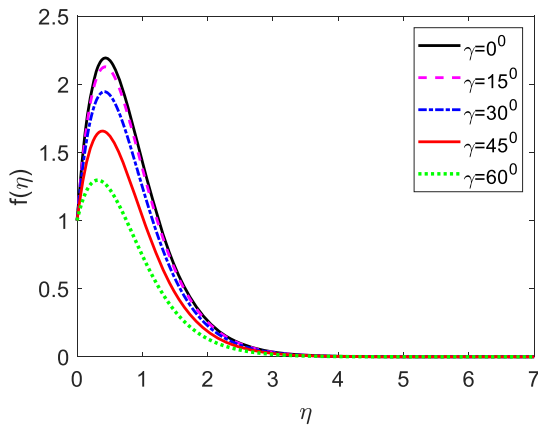


Fig. 7. Velocity profile for (γ).

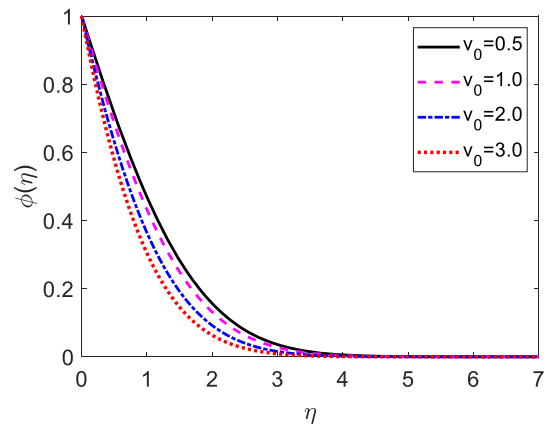


Fig. 10. Concentration profile for (v_0).

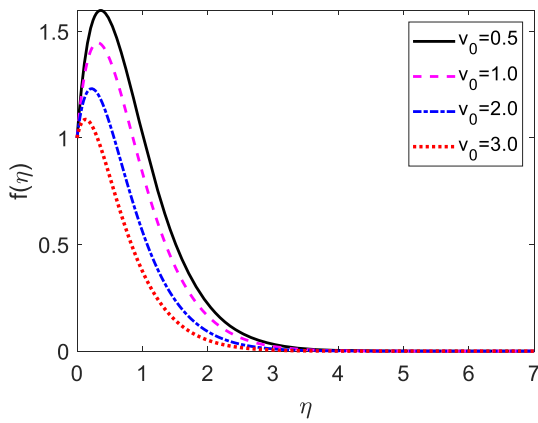


Fig. 8. Velocity profile for (v_0).

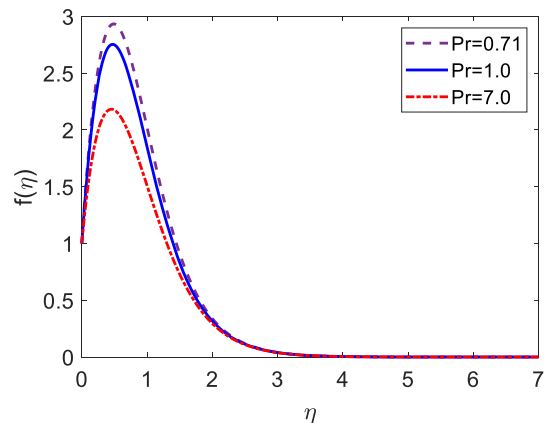


Fig. 11. Velocity profile for (Pr).

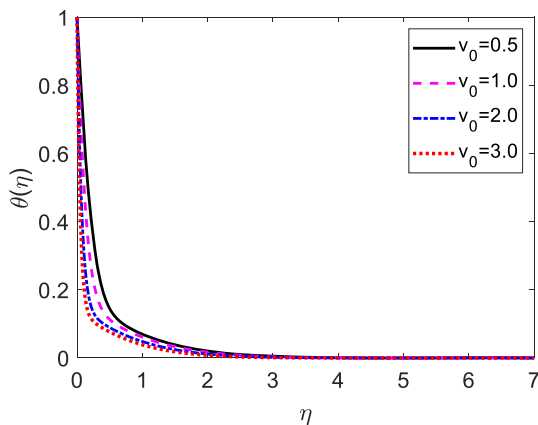


Fig. 9. Temperature profile for (v_0).

the analysis as long as the other parameters or numbers are held constants. So, when a magnetic field is applied to a flow field, a Lorentz force is created, which in turn makes a lessening in the fluid's speed away from the sheet surface. As a consequence, the values of $f(0)$ lessen at the wall for rising values of M .

Fig. 7 elucidates the velocity distribution for several amounts of the inclination angle (γ). The fluid velocity is diminished for mounting quantities of γ . The fluid has higher motion when the porous plate is vertical ($\gamma = 0^\circ$) than when the plate is at an inclined position. On the contrary, the fluid's movement goes down for mounting amounts of γ . The local skin friction coefficient lessened by around 12 % owing to

growing values of γ from 15° and 30° . This is the reason that the buoyancy effect owing to the gravity component ($g\cos\gamma$) is reduced, as the sheet is inclined.

The velocity curves for several amounts of suction parameter (v_0) are shown in Fig. 8. This Figure describes how the decrease in the non-dimensional fluid velocity enlarges the values because the momentum boundary layer thickness is enhanced. When we sucked some fluid from the computational domain, then the fluid particles won't be able to travel freely. Therefore, the viscous force improves for growing amounts of v_0 . By raising the amount of v_0 (1.0–3.0), the local skin friction coefficient falls by around 27 %. The suction parameter demonstrates the common reality that the suction stops the boundary layer expansion. Fig. 9 discusses the temperature curves for several amounts of v_0 . The fluid temperature diminishes for improving quantities of v_0 as shown in Fig. 9. Also, it is shown in Table 5 that growing values of v_0 (1.0–3.0) enhance the heat transmission rate by about 66 %. Hence the heat is transferred quickly from the porous plate with v_0 . The impact of v_0 on the concentration curves is revealed in Fig. 10. The concentration function goes down for rising values of v_0 . Table 5 shows that the mass transmission rate augments by about 49 % for growing amounts of v_0 (1.0–3.0). This is because applying suction has the propensity to make the concentration boundary layer thinner.

The disparity of the non-dimensional temperature contrary to η for different amounts of Prandtl number (Pr) is expressed in Fig. 11. This is well established that Pr is the ratio of kinematic viscosity to thermal conductivity. We have the mathematical formula for Pr as $Pr = \frac{\rho\nu C_p}{k}$. The kinematic viscosity varies as Pr . When the values of Pr improve, at that time the kinematic viscosity goes up. The frictional force increases the kinematic viscosity as it occurs in the computational domain. Mounting

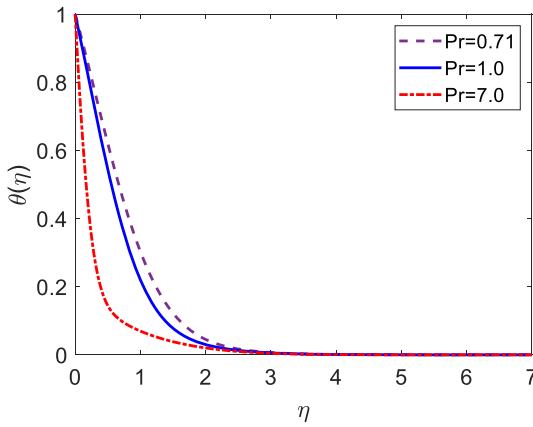


Fig. 12. Temperature profile for (Pr).

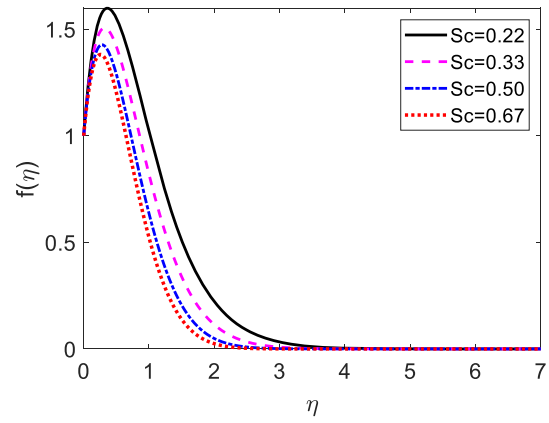


Fig. 15. Velocity profile for (Sc).

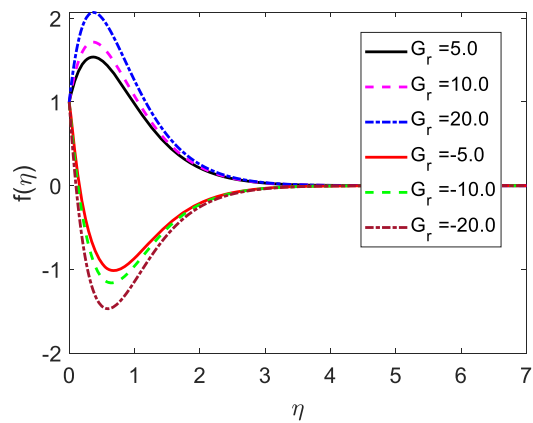


Fig. 13. Velocity profile for (G_r).

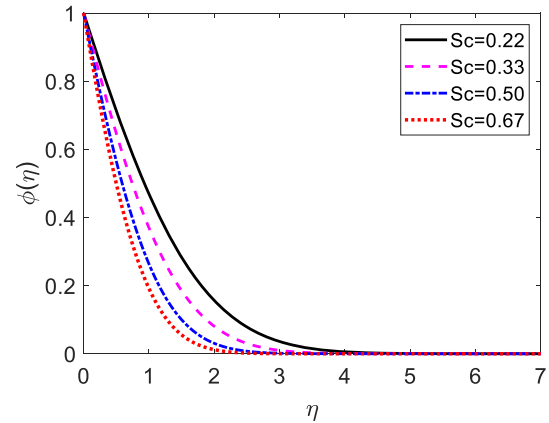


Fig. 16. Concentration profile for (Sc).

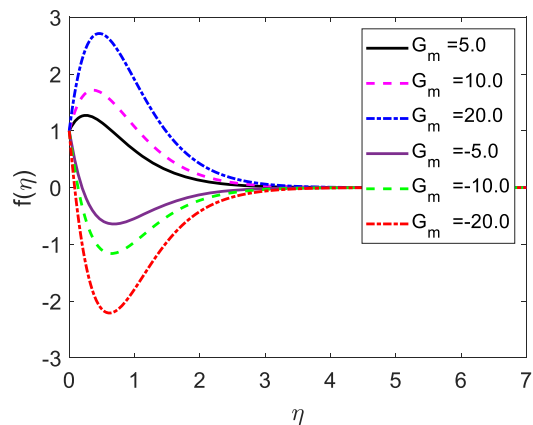


Fig. 14. Velocity profile for (G_m).

quantities of Pr, results in a decrease in the local skin friction coefficient. This coefficient goes down by around 16 % owing to improving amounts of Pr from 1.0 to 7.0. As a result, the fluid velocity falls quickly for improving amounts of Pr. The fluid kinematic viscosity advances making it considerably thicker owing to enhancing the values of Pr. Besides, the non-dimensional temperature field for various amounts of Pr is demonstrated in Fig. 12. It is common knowledge that the thermal conductivity and the Prandtl number (Pr) change inversely with one another. According to the above concept, the thermal conductivity reduces for mounting amounts of Pr. The rate of heat transmission for Pr improves as the thermal conductivity decays. When the Prandtl number

is raised from 1.0 to 7.0, the rate of heat transmission improves by approximately 236 %. As a result, the fluid temperature goes down quickly for uplifting amounts of Pr as revealed in Fig. 12. This is because fluid with high amounts of Pr has a high heat capacity, which improves heat transfer.

Fig. 13 illustrates the velocity field for various amounts of the local Grashof number (G_r). Fig. 13 indicates that the fluid velocity enhances for growing quantities of G_r . Both negative and positive values of G_r result in the velocity field having a symmetrical structure. The symmetrical shape of the velocity field is observed for negative and positive values of G_r . The system is heating for $G_r > 0$. On the other hand, the system is cooling for $G_r < 0$. The same behavior is observed for several amounts of the modified local Grashof number (G_m) as revealed in Fig. 14.

The velocity field for changes in Schmidt number (Sc) is depicted in Fig. 15. The kinematic viscosity changes along with the Schmidt number. The kinematic viscosity enhances for growing values of Sc. The kinematic viscosity enhances, which means that the frictional force improves in the computational region. Because of this, the fluid particles are unable to move independently within the computational domain. Besides, the local skin friction coefficient lessens by approximately 7 % owing to growing amounts of Sc from 0.33 to 0.67. As a result, the fluid motion decays for uplifting values of Sc. This is because, as illustrated in Fig. 15, the flow field experiences a drop in velocity at all points when heavier diffusing species are present. The concentration field for several amounts of Sc is described in Fig. 16. The Schmidt number and molecular (species) diffusivity are known to be inversely correlated. The mass transfer rate enhances about by 52 % owing to growing values of Sc from 0.33 to 0.67. Therefore, a rise in Sc causes the species concentration to

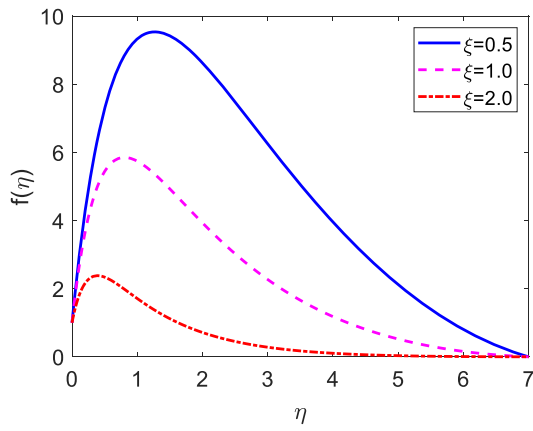


Fig. 17. Velocity profile for (ξ).

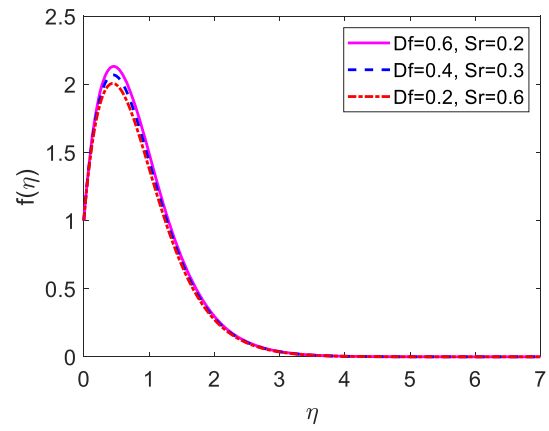


Fig. 20. Velocity profile for Df and Sr.

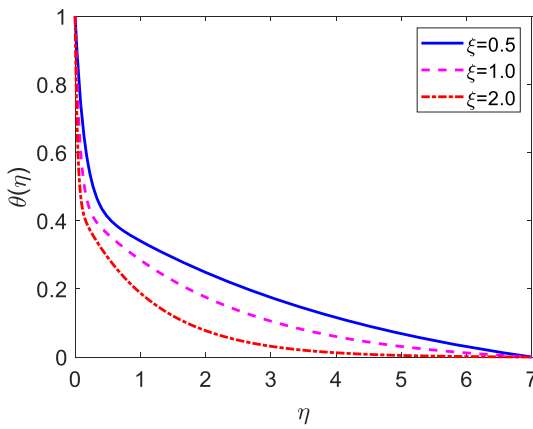


Fig. 18. Temperature profile for (ξ).

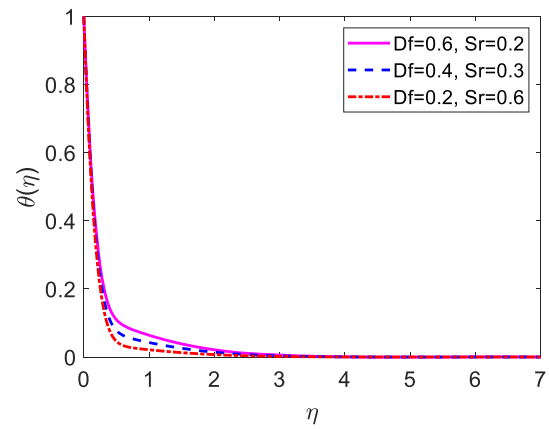


Fig. 21. Temperature profile for Df and Sr.

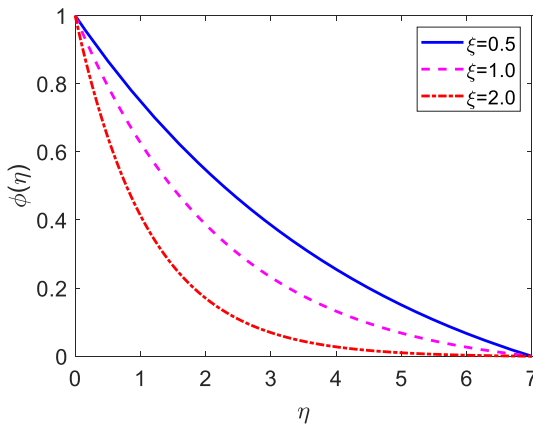


Fig. 19. Concentration profile for (ξ).

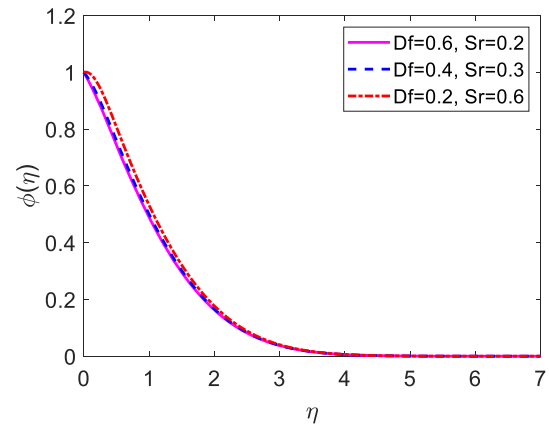


Fig. 22. Concentration profile for Df and Sr.

drop more quickly.

The effect of the unsteady parameter (ξ) on the velocity, temperature and concentration profiles are shown in Figs. 17–19, respectively. The velocity, temperature, and concentration decay for higher values of the unsteady parameter.

The influence of Dufour number (Df) and Soret number (Sr) on the velocity, temperature, and concentration fields are shown in Figs. 20–22, respectively. Quantitatively, Df decreases from 0.6 to 0.2 (Sr increases from 0.2 to 0.6), the fluid velocity and temperature decrease but the concentration of the fluid enhances for this case.

Fig. 23 shows the Nusselt number (Nu) for various values of the suction parameter (v_0). It is clearly observed from Fig. 23 that the Nusselt number increases for higher values of the suction. It means the heat transfer rate enhances for this situation. For this reason, the fluid temperature diminishes for v_0 . The effects of the different values of the inclination (γ) on the skin-friction is displayed in Fig. 24. The skin-friction reduces for higher values of the inclined angle (γ). It means the frictional force is more active for higher values γ . For this reason, the velocity of the fluid reduces for higher values of γ .

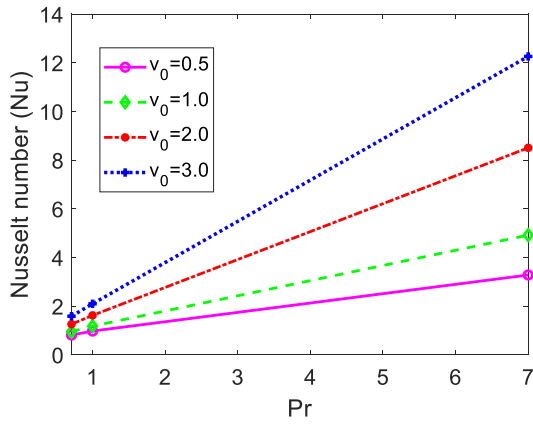


Fig. 23. Nusselt number (Nu) for v_0 .



Fig. 24. Skin-friction (C_f) for γ .

Table 1
Numerical values of $-\theta'(0)$, $f(0)$, and $-\phi'(0)$ for various amounts of D_f .

D_f	$f(0)$	$-\theta'(0)$	$-\phi'(0)$
0.5	3.90866044226245	4.34542061388490	0.601216552803069
1.0	4.08719307953796	3.60339399555823	0.601216552803069
2.0	4.67069113120348	1.39576300308372	0.601216552803069
3.0	5.96082900134952	0.99404855720680	0.601216552803069

Table 2
Numerical values of $-\theta'(0)$, $f(0)$, and $-\phi'(0)$ for various amounts of Pr.

Pr	$f(0)$	$-\theta'(0)$	$-\phi'(0)$
0.71	6.06446499287058	0.705806866403232	0.601216552803069
1.0	5.71714148619972	0.878070788488454	0.601216552803069
7.0	4.08719307953796	3.60339399555823	0.601216552803069

5. Local skin friction coefficient, heat, and mass transfer rates

The researchers are very much interested in explaining not only the fluid flow but also the local heat transmission rate ($-\theta'(0)$), skin friction coefficient ($f(0)$), and mass transmission rate ($-\phi'(0)$). The following Tables give us the amounts of $f(0)$, $-\theta'(0)$ and $-\phi'(0)$ at the plate for several quantities of the non-dimensional parameters or numbers. For various amounts of the dimensionless parameters or numbers, the values of $f(0)$, $-\theta'(0)$, and $-\phi'(0)$ at the plate are provided in the following Tables.

Table 1 presents the mass transmission rate ($-\phi'(0)$), the local skin friction coefficient ($f(0)$), and the heat transmission rate ($-\theta'(0)$) at the

Table 3
Numerical values of $-\theta'(0)$, $f(0)$, and $-\phi'(0)$ for various values of γ .

γ	$f(0)$	$-\theta'(0)$	$-\phi'(0)$
0^0	4.31522485212344	3.60339399555823	0.601216552803069
15^0	4.08719307953796	3.60339399555823	0.601216552803069
30^0	3.44218892272492	3.60339399555823	0.601216552803069
45^0	2.40627315567501	3.60339399555823	0.601216552803069
60^0	1.05762810051579	3.60339399555823	0.601216552803069

Table 4
Numerical values of $-\theta'(0)$, $f(0)$, and $-\phi'(0)$ for various amounts of Sc.

Sc	$f(0)$	$-\theta'(0)$	$-\phi'(0)$
0.22	4.08719307953796	3.60339399555823	0.601216552803069
0.33	3.81242682724481	3.60339399555823	0.756769634209805
0.50	3.55656922496316	3.60339399555823	0.963553979415748
0.67	3.39722515877667	3.60339399555823	1.14691830107513

Table 5
Numerical values of $-\theta'(0)$, $f(0)$, and $-\phi'(0)$ for various amounts of v_0 .

v_0	$f(0)$	$-\theta'(0)$	$-\phi'(0)$
0.5	4.08719307953796	3.60339399555823	0.601216552803069
1.0	3.56430299768720	6.38637576923659	0.676806130134389
2.0	2.61795753327089	12.3376561273991	0.837546383783995
3.0	1.62096819762152	18.4746650223649	1.00899835593378

surface with the Dufour number (D_f). Table 1 makes it evident that while the Dufour number improves local skin friction at the plate, it lowers the rate of heat transmission. The amount of $f(0)$ enhances by 52 % and the amount of $-\theta'(0)$ reduces by 77 % due to moving values of D_f from 0.5 to 3.0.

Table 2 illustrates the properties of several amounts of Pr on the mass transmission rate ($-\phi'(0)$), the local skin friction coefficient ($f(0)$), and the heat transmission rate ($-\theta'(0)$) at the surface. Table 2 displays that while the Prandtl number enhances the heat transmission rate at the plate, it lessens the local skin friction coefficient. The local skin friction is reduced by 32 % and the heat transmission rate is enhanced by 410 % due to moving values of Pr from 0.71 to 1.0.

Table 3 shows the mass transmission rate ($-\phi'(0)$), the local skin friction coefficient ($f(0)$), and the heat transmission rate ($-\theta'(0)$) at the surface in the presence of the inclination of the porous plate (γ). The inclination of the porous plate lowers the local skin friction coefficient at the plate, as demonstrated in Table 3. The values of $f(0)$ enhance by 75 % due to moving values of γ from 0^0 to 60^0 .

The features of the Schmidt number (Sc) on the mass transmission rate ($-\phi'(0)$), the local skin friction coefficient ($f(0)$), and the heat transmission rate ($-\theta'(0)$) at the surface are displayed in Table 4. The mass transmission rate goes up and the local skin friction coefficient falls as the Schmidt number grows, as inferred from Table 4. As Sc climbs from 0.22 to 0.50, the coefficient of local skin friction reduces by around 13 % and the heat transmission rate rises by 60 %, respectively.

Table 5 expresses the mass transmission rate ($-\phi'(0)$), the local skin friction coefficient ($f(0)$), and the heat transmission rate ($-\theta'(0)$) at the plate for different amounts of the suction parameter (v_0). The values of $f(0)$ reduce but the amounts of $-\theta'(0)$ and $-\phi'(0)$ augment for uplifting values of v_0 . The values of $f(0)$ diminish by about 55 % but enhance the

Table 6
Numerical values of $-\theta'(0)$, $f(0)$, and $-\phi'(0)$ for various amounts of M.

M	$f(0)$	$-\theta'(0)$	$-\phi'(0)$
0.5	4.08719307953796	3.60339399555823	0.601216552803069
1.5	3.34326688978145	3.60339399555823	0.601216552803069
3.0	2.46159168112501	3.60339399555823	0.601216552803069
4.0	1.97912051408047	3.60339399555823	0.601216552803069

Table 7Numerical values of $-\theta'(0)$, $f(0)$, and $-\varphi'(0)$ for various amounts of G_r .

	G_m	$f(0)$	$-\theta'(0)$	$-\varphi'(0)$
5.0	10.0	3.16671717519131	3.60339399555823	0.601216552803069
10.0	10.0	4.08719307953796	3.60339399555823	0.601216552803069
20.0	10.0	5.92814488825044	3.60339399555823	0.601216552803069
-5.0	-10.0	-7.56665447776200	3.60339399555823	0.601216552803069
-10.0	-10.0	-8.48713038211104	3.60339399555823	0.601216552803069
-20.0	-10.0	-10.3280821907958	3.60339399555823	0.601216552803069

Table 8Values of $-\theta'(0)$ and $-\varphi'(0)$ for ν_0 and D_f .

	D_f	$-\theta'(0)$ Hasanuzzaman et al. [14]	$-\theta'(0)$ Present study	$-\varphi'(0)$ Hasanuzzaman et al. [14]	$-\varphi'(0)$ Present study
0.5	0.2	1.41983	1.49929	0.22187363	0.19355095030467
0.5	0.5	1.48232	1.36665	0.13702065	0.13355095030862

Table 9Values of $-\theta'(0)$ and $-\varphi'(0)$ for Pr and Sc .

Pr	Sc	$-\theta'(0)$	$-\theta'(0)$	$-\varphi'(0)$	$-\varphi'(0)$
		Hasanuzzaman et al. [14]	Present study	Hasanuzzaman et al. [14]	Present study
0.71	0.22	1.40316	1.39423	0.24471	0.26012
1.0	0.22	1.82297	1.83429	0.28981	0.27012
0.71	0.60	1.41983	1.39666	0.22187	0.17355
0.71	0.75	1.42843	1.42102	0.17101	0.16977

values of $-\theta'(0)$ by about 189 % and $-\varphi'(0)$ by 49 % due to moving values of ν_0 from 1.0 to 3.0. Consequently, the fluid flow, temperature, and concentration functions are reduced owing to increasing values of ν_0 .

The mass transmission rate ($-\varphi'(0)$), the local skin friction coefficient ($f(0)$), and the heat transmission rate ($-\theta'(0)$) at the surface for various amounts of the magnetic force parameter (M) are discussed in Table 6. The values of $f(0)$ reduced about by 51 % due to increasing values of M from 0.5 to 4.0. The values of $-\theta'(0)$ and $-\varphi'(0)$ are fixed for M . As a result, the fluid motion falls quickly owing to an increase in M .

Table 7 expresses the influences of several amounts of the local Grashof number (G_r) on the mass transmission rate ($-\varphi'(0)$), the local skin friction coefficient ($f(0)$), and the heat transmission rate ($-\theta'(0)$) at the surface. We have noted from Table 7 that the amounts of $-\theta'(0)$ and $-\varphi'(0)$ are fixed for G_r . The values of $f(0)$ reduce about by 45 % due to increasing values of G_r from 10.0 to 20.0. As a consequence, the velocity function slows down quickly owing to an increase in G_r .

6. Comparable tables

The numerical result of the existing research has been compared with previously published work which is included in Tables (8 and 9). Numerical outcomes for the amounts of the heat transmission rate at the plate are compared with the findings of Hasanuzzaman et al. [14] for the case of ($\gamma = 0^0$) to confirm the validity and correctness of the result obtained.

7. Conclusions

The characteristics of the Dufour and thermal diffusion on a time-dependent free magneto-convective heat-mass transfer flow through an inclined permeable plate are examined in this research by applying the finite difference method. The present simulations bring out the following conclusions:

- The values of $f(0)$ enhance by 75 % due to moving values of γ from 0^0 to 60^0 .

- The fluid velocity upgrades for improving amounts of D_f and S_r .
- The temperature function falls for Pr but enhances for D_f .
- The concentration function goes down for Sc but improves for S_r .
- The values of $f(0)$ reduced about by 51 % due to increasing values of M from 0.5 to 4.0.
- The amount of $f(0)$ enhances by 52 % and the amount of $-\theta'(0)$ reduces by 77 % due to moving values of D_f from 0.5 to 3.0.
- Especially, the results are excellently consistent with the research that was published earlier.

The outcome of this study could be useful in a variety of fields, astrophysics, and geophysics for example the cooling towers, boundary layer control in aerodynamics, nuclear reactors cooling, and more.

CRediT authorship contribution statement

Md. Hasanuzzaman: Writing – review & editing, Supervision, Software, Resources, Project administration, Investigation, Funding acquisition, Conceptualization. **Mahamudul Hassan Milon:** Writing – review & editing, Writing – original draft, Visualization, Validation, Software, Methodology, Formal analysis, Data curation. **Md. Mosharraf Hossain:** Writing – original draft, Visualization, Validation, Software, Methodology, Investigation, Formal analysis, Data curation, Conceptualization. **Md. Asaduzzaman:** Writing – original draft, Visualization, Software, Methodology, Formal analysis, Data curation, Conceptualization.

Declaration of competing interest

The authors declare that they have no known competing financial interests or personal relationships that could have appeared to influence the work reported in this paper.

Data availability

The authors do not have permission to share data.

References

- [1] A. Umemura, C.K. Law, Natural-convection boundary-layer flow over a heated plate with arbitrary inclination, *J. Fluid Mech.* 219 (1990) 571–584.
- [2] M.A. Hossain, D.A.S. Rees, I. Pop, Free convection-radiation interaction from an isothermal plate inclined at a small angle to the horizontal, *Acta Mech.* 127 (1) (1998) 63–73.
- [3] M. Anghel, M.A. Hossain, S. Zeb, I. Pop, Combined heat and mass transfer by free convection past an inclined flat plate, *Int. J. Appl. Mech. Eng.* 6 (2) (2001) 473–487.
- [4] C.H. Chen, Heat and mass transfer in MHD flow by natural convection from a permeable, inclined surface with variable wall temperature and concentration, *Acta Mech.* 172 (3) (2004) 219–235.

- [5] M.S. Alam, M.M. Rahman, M.A. Sattar, MHD-free convective heat and mass transfer flow past an inclined surface with heat generation, *Sci. Technol. Asia* (2006) 1–8.
- [6] G.M. Reddy, Lie group analysis of heat and mass transfer effects on steady MHD free convection dissipative fluid flow past an inclined porous surface with heat generation, *Theor. Appl. Mech.* 39 (3) (2012) 233–254.
- [7] F. Ali, I. Khan, S. Shafie, Conjugate effects of heat and mass transfer on MHD free convection flow over an inclined plate embedded in a porous medium, *PLoS ONE* 8 (6) (2013) e65223.
- [8] E.R.G. Eckert, R.M. Drake Jr, *Analysis of Heat and Mass Transfer*, McGraw-Hill Book Company, New York, 1972.
- [9] Z. Dursunkaya, W.M. Worek, Diffusion-thermo and thermal-diffusion effects in transient and steady natural convection from a vertical surface, *Int. J. Heat Mass Transf.* 35 (8) (1992) 2060–2065.
- [10] N.G. Kafoussias, E.W. Williams, Thermal-diffusion and diffusion-thermo effects on mixed free-forced convective and mass transfer boundary layer flow with temperature-dependent viscosity, *Int. J. Eng. Sci.* 33 (9) (1995) 1369–1384.
- [11] A. Postelnicu, Influence of chemical reaction on heat and mass transfer by natural convection from vertical surfaces in porous media considering Soret and Dufour effects, *Heat Mass Transf.* 43 (6) (2007) 595–602.
- [12] M.S. Alam, Effect of Thermophoresis on MHD free convective heat and mass transfer flow along an inclined stretching sheet under the influence of Dufour-Soret effects with variable wall temperature, *Sci. Technol. Asia* (2016) 46–58.
- [13] B. Prabhakar Reddy, O.D. Makinde, Numerical study on MHD radiating and reacting unsteady slip flow past a vertical permeable plate in a porous medium, *Int. J. Ambient Energy* 43 (1) (2022) 6007–6016.
- [14] Sreedevi, G., Rao, D.R.V., Makinde, O.D., & Reddy, G., (2017). Soret and Dufour effects on MHD flow with heat and mass transfer past a permeable stretching sheet in the presence of thermal radiation.
- [15] H. Mondal, D. Pal, S. Chatterjee, P. Sibanda, Thermophoresis and Soret-Dufour on MHD mixed convection mass transfer over an inclined plate with non-uniform heat source/sink and chemical reaction, *Ain Shams Eng. J.* 9 (4) (2018) 2111–2121.
- [16] M. Hasanuzzaman, M.A. Kabir, M.T. Ahmed, Transpiration effect on unsteady natural convection boundary layer flows around a vertical slender body, *Results. Eng.* 12 (2021) 100293.
- [17] M. Hasanuzzaman, M. Azad, A. Kalam, M. Hossain, Effects of Dufour and thermal diffusion on unsteady MHD free convection and mass transfer flow through an infinite vertical permeable sheet, *SN. Appl. Sci.* 3 (12) (2021) 1–11.
- [18] M. Hasanuzzaman, T. Ahamed, A. Miyara, Thermal radiation effect on unsteady magneto-convective heat-mass transport passing in a vertical permeable sheet with chemical reaction, *Comput. Math. Methods Med.* (2022) 2022.
- [19] M. Hasanuzzaman, S. Sharin, T. Hassan, M.A. Kabir, R. Afroj, A. Miyara, Unsteady magneto-convective heat-mass transport passes in a vertical permeable sheet with an internal heat generation effect, *Transp. Eng.* 9 (2022) 100126.
- [20] S.I. Pai, *Magnetogasdynamics and Electromagnetogasdynamics*. In *Magnetogasdynamics and Plasma Dynamics*, Springer, Vienna, 1962, pp. 27–40.
- [21] J.C. Ali, E.A. Sameh, S.A. Abdulkareem, Melting and radiation effects on mixed convection from a vertical surface embedded in a non-Newtonian fluid saturated non-Darcy porous medium for aiding and opposing external flows, *Int. J. Phys. Sci.* 5 (7) (2010) 1212–1224.
- [22] W.T. Cheng, C.H. Lin, Unsteady mass transfer in mixed convective heat flow from a vertical plate embedded in a liquid-saturated porous medium with melting effect, *Int. Commun. Heat Mass Transf.* 35 (10) (2008) 1350–1354.